LASER
& PHOTONICS
REVIEWS

Laser Photonics Rev. **9,** No. 5, 530–537 (2015) / **DOI** 10.1002/lpor.201500089

ORIGINAL
PAPER

Abstract Directional side scattering of light by individual gold nanoparticles (AuNPs) trimers assembled by the atomic force microscope (AFM) nanomanipulation method is investigated in experiment and theory. The AFM nanomanipulation approach brings an active way to construct ultracompact and effective optical nanoantennas. Different configurations of the trimers are constructed in situ via AFM nanomanipulation. Unidirectional side scattering of light by a single trimer is demonstrated with a broad response bandwidth over 400 nm and directivity up to ~7.8 dB in experiments. The near-field plasmon coupling of the AuNPs is simulated with the 3D finite-difference time-domain method and the far-field radiation patterns are calculated by employing near-field-to-far-field transformation methods. The calculated results are in agreement with the experiments qualitatively. The physical origin is revealed intuitively by employing a simple phenomenological "two-dipole" model. The unidirectional light scattering is due to the interference between multiple plasmonic resonance modes of the trimers. The study contributes to the understanding of the optical response of complex nanostructures and optimizing nanoantenna performances for practical applications, e.g. increasing the detection efficiency of surface-enhanced spectroscopy.

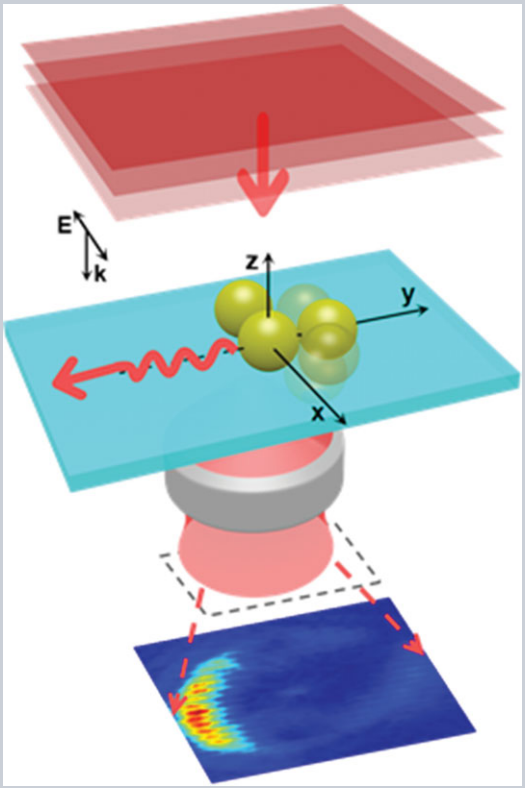

Directional side scattering of light by a single plasmonic trimer

Guowei Lu[1,2,*], Yuwei Wang[1], R. Yuanying Chou[1], Hongming Shen[1], Yingbo He[1], Yuqing Cheng[1], and Qihuang Gong[1,2]

1. Introduction

Metallic nanostructures associated with collective oscillation of free electrons possess unique optical properties to route and manipulate light at nanoscale dimensions [1–3]. This unprecedented ability has allowed for rapid advances in many interdisciplinary subjects, such as biological sensing, surface-enhanced spectroscopy, nanoscale all-optical devices, etc. [4–7]. Compared with individual metallic nanoparticles, assembled plasmonic nanostructures provide a more effective way to control light or manipulate light–matter interaction at nanoscale dimensions. For instance, a dimer consisting of two simple spherical nanoparticles can concentrate light within its gap efficiently [8–10]. Also, optical trapping as well as the optical manipulation have been used to build composited nanoassemblies [11–13]. The nanoantenna coupled to a miniature metallic grating can be engineered to enhance the light emission intensity and narrow the emission directivity [14–17]. Assembling metallic nanoparticles as plasmonic oligomers, i.e. artificial molecules, has given rise to many interesting collective behaviors beyond individual nanoparticles [18–24].

Up to now, most of the plasmonic nanoassemblies have been investigated for surface-enhanced Raman scattering, surface-enhanced fluorescence, scattering spectroscopy, and polarization control of light emission etc [25–28]. Additionally, the plasmonic antenna can also reshape the light emission angular distribution, which is helpful to improve detection efficiency [29–31]. Recently, directional scattering has been demonstrated in a single-element nano-object in theory and experiment, such as metallic core–shell nanoparticles [32, 33], nanocups [34], V-shape

[1] State Key Laboratory for Mesoscopic Physics, Department of Physics, Peking University, Beijing, 100871, China
[2] Collaborative Innovation Center of Quantum Matter, Beijing, 100871, China
*Corresponding author: e-mail: guowei.lu@pku.edu.cn

© 2015 by WILEY-VCH Verlag GmbH & Co. KGaA, Weinheim

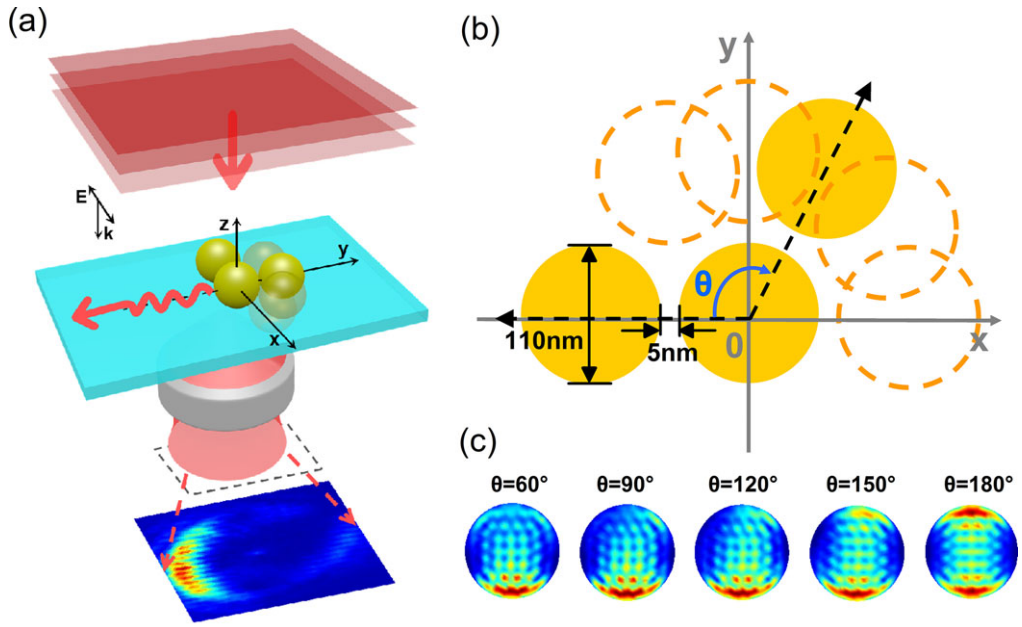

Figure 1 (a) Schematic design of directional scattering by plasmonic trimer. Side scattering directionality is obtained when the incident light polarizes along one side of the trimer. (b) Illustration of the designed plasmonic trimer nanostructure with the different angles. (c) Simulated scattering patterns as the intersection angle varies from 60° to 180°.

antennas [35] and nonmetallic silicon nanoparticles [36]. Using nanometer localized asymmetrical excitation by an electron beam, directional emissions were also obtained for individual symmetrical gold nanodisks, nanoholes, and truncated bitetrahedrons [37–39]. To obtain directed light emission, the design strategies rely on the interference of multiple plasmon resonant modes through carefully designing spatial separation and phase differences [40]. The nanoassembly of the metal nanoparticles is able to control the light-emission direction if the mirror symmetry of the nanoassembly is broken relative to the light polarization. A well-known plasmonic nanoassembly to favor emission unidirectionality is the Yagi–Uda antenna consisting of several nanorods with different sizes arranged as an analog of radiative antenna [41–44]. Until now, most of the plasmonic nanoassemblies for light directivity control are obtained through the top-down nanofabrication techniques in which the nanostructures are fixed after the fabrication. As a result, numerous test samples are necessary to investigate different configurations. On the other hand, the bottom-up colloidal AuNPs have been studied for over 100 years and have been used as building blocks to construct various plasmonic complexes recently [11–13, 15]. However, directional scattering of light by the nanoassemblies of the AuNPs is seldom reported.

In this study, plasmonic oligomers are assembled with the AuNPs by using the AFM nanomanipulation method and the configurations can be adjusted in situ, which is convenient for studying the optical response of the antenna. Unidirectional side scattering by different trimers is achievable with a broad response bandwidth over 400 nm and directivity up to ∼7.8 dB. The directional scattering properties are also calculated with the finite-difference time-domain (FDTD) method and the numerical results are in good agreement with the experiments. The directional scattering can be explained by the plasmonic coupling of neighboring AuNPs resulting in multiple plasmon resonance modes with different phase, the interference of which leads to the unidirectional scattering. A simple intuitive "two-dipole" model is applied to visualize the physical picture successfully. Our observations of the trimer should contribute to understanding surface-enhanced spectroscopy due to the colloid aggregations that could also modify the emission directions.

2. Directional scattering by plasmonic trimer in theory

Directional emissions due to the far-field interference of multiple resonant modes have already been reported [37–40]. Analogically, the nanoassembly of several identical AuNPs should also be able to control the light-scattering direction if the mirror symmetry of the nanoassembly is broken relative to the light polarization. At first, through introducing symmetry-broken, unidirectional side scattering of light by a right-triangle-like trimer is feasible, as shown in Fig. 1 by numerical simulations. Figure 1a concisely presents the design of directional light scattering by a trimer consisting of three AuNPs with diameters of ∼110 nm. When the polarization of the incident light is

© 2015 by WILEY-VCH Verlag GmbH & Co. KGaA, Weinheim

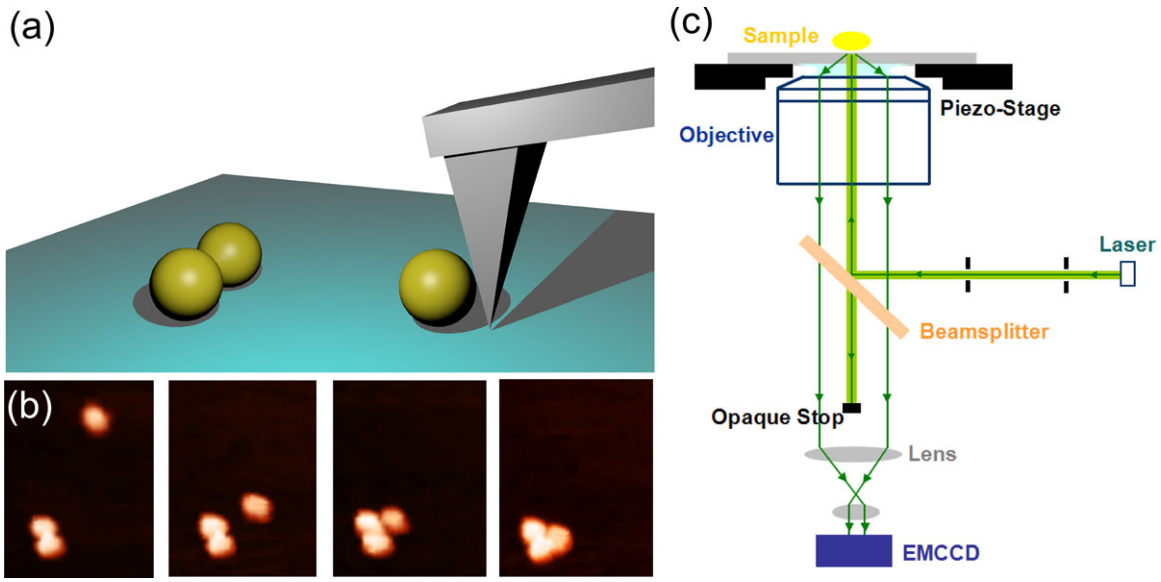

Figure 2 AFM nanomanipulation and scattering pattern measurement of the gold nanoparticles oligomer. (a) Illustration of AFM manipulation method. (b) Representative AFM images at different stages in the assembly process. (c) Schematic diagram of the optical system for scattering-pattern measurement.

along one side of the trimer, unidirectional side scattering appears. By changing the intersection angle θ ranging from 60° to 180°, as illustrated in Fig. 1b, the calculated scattering patterns present significant unidirectional scattering for the asymmetric trimers, as shown in Fig. 1c. This can be understood by the plasmonic coupling of neighboring AuNPs resulting in multiple plasmon resonance modes with different phase at specific wavelengths. Also, the interaction of multiple electric plasmonic resonance modes would lead to the instructive or destructive interference of the scattering light in the far-field.

3. Material and methods

To construct the plasmonic oligomer at will, we used the AFM nanomanipulation method to control the positions of the AuNPs on the substrate surface. The AFM nanomanipulation method allows us to rearrange the AuNPs and modify nanostructures in situ as the schematic procedure in Fig. 2a shows, which is an active way to investigate the optical response of the plasmonic oligomer with different configurations. Although the position accuracy of the AuNPs in the assembled nanostructures is inherently limited, the AFM nanomanipulation has enabled the realization of novel hybrid structures of semiconductor or metallic nanoparticles [45–48]. When the near-field coupling within the plasmonic oligomer is considered, the atomic-level flatness surface of the metallic components may be particularly crucial. So, in the present study, we used AuNPs synthesized by the wet chemical citrate reduction method [49]. The synthesized AuNPs with diameter of ~110 nm were immobilized on the glass coverslip [50]. At first, the AFM was operated in semicontact mode to image and identify the location of the AuNPs. Then, we employed the AFM in contact mode to push the particles to the target positions to construct the required plasmonic oligomers. To demonstrate the assembly process intuitively, three representative AFM images at different assembling stages are shown in Fig. 2b. Therefore, the AFM manipulation can be applied for assembling and controlling the oligomer configurations in a convenient way.

The *sp*-band free electrons of the gold nanostructures are driven by the external light presenting a collective oscillation. This oscillation results in an induced dipole moment that usually radiates the power as scattering light. So, it is possible to route and manipulate the radiation direction by the plasmonic nanostructures based on the interference of different plasmon resonant modes. In order to investigate the directional scattering of light, the momentum-space images are recorded at the back focal plane of the objective lens with a charge-coupled device (CCD) camera. Figure 2c shows the schematic design of angular radiation pattern measurements. The laser beam at $\lambda = 532$ nm or 633 nm initially went through the objective lens with a small beam diameter resulting in a low effective numerical aperture. The light scattered by the plasmonic nanostructure was collected by the same objective. To suppress the reflected light from the nanostructures and interface directly, an opaque stop was placed in front of the tube lens. The scattering light is less influenced by the beam stop since most of the scattering light is emitted around the critical angle [51–57]. By placing a CCD appropriately at the Fourier plane of the objective lens, we successfully obtained the scattering radiation pattern. The scattering pattern at the back focal plane can be used as a map of angular emission distribution due to the nanostructures [50, 51].

© 2015 by WILEY-VCH Verlag GmbH & Co. KGaA, Weinheim

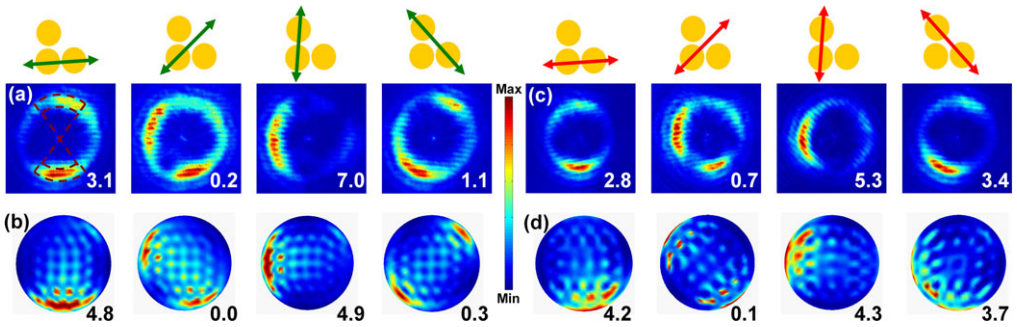

Figure 3 Experimental (a), (c) and simulated (b), (d) scattering patterns illuminated by 532-nm laser (a), (b) and 633-nm laser (c), (d), respectively, with different incident-light polarization as indicated by the double arrows. The directivity values are also indicated correspondingly for comparison, and the unit dB is omitted for simplicity.

4. Results and discussion

First, to set the scene, the light-scattering patterns of a single AuNP and dimer were investigated in detail (supporting information). Due to the symmetrical shape of the monomers and the dimers, both the experimental and theoretical results confirm that there is no unidirectional scattering, and this is consistent with the previous conclusions [51]. To obtain unidirectional scattering, three AuNPs were assembled to form a trimer to break the symmetry, and the corresponding AFM image is shown in Fig. 2b. The experimental and corresponding simulated scattering patterns of such an asymmetric plasmonic trimer are shown in Fig. 3, which are illuminated at wavelengths of 532 nm and 633 nm, respectively. For the case of 532 nm, an obvious unidirectional scattering occurs when the incident light polarizes along one side of the right-triangle-like trimer, as shown in the 1st and 3rd picture of Fig. 3a. In these situations, we obtain directional side scattering that is nearly perpendicular to the incident light polarization. In the 2nd picture, when the light polarization is parallel to the symmetry axis of the right-triangle-like trimer, the scattering intensity distribution presents two symmetric lobes without directional scattering features. When the polarization is along the hypotenuse of the trimer, the scattering pattern still presents unidirectionality to some extent, yet the contrast is relatively weak compared with the 1st and 3rd cases. To quantitatively characterize the directionality scattering of the trimer, the directivity is defined here, i.e., a decibel comparison of the side scattering light intensity in the opposite direction respective to the light polarization. This expression is indicated in following simplified formula: $\text{Directivity} = 10\log\frac{\sum I_{\text{Sca}}^{\text{Left}}}{\sum I_{\text{Sca}}^{\text{Right}}}$. The directivities are obtained by integrating the scattering intensity over two opposite intervals shown in the 1st picture of Fig. 3a (dark red dashed line). The quantitative values are indicated in Fig. 3 for experiment and simulation, respectively. Specifically, we get an experimental directivity ~7.0 dB in the *y*-direction when the incident light at $\lambda = 532$ nm is polarized along one side of the trimer as shown in the 3rd case of Fig. 3a.

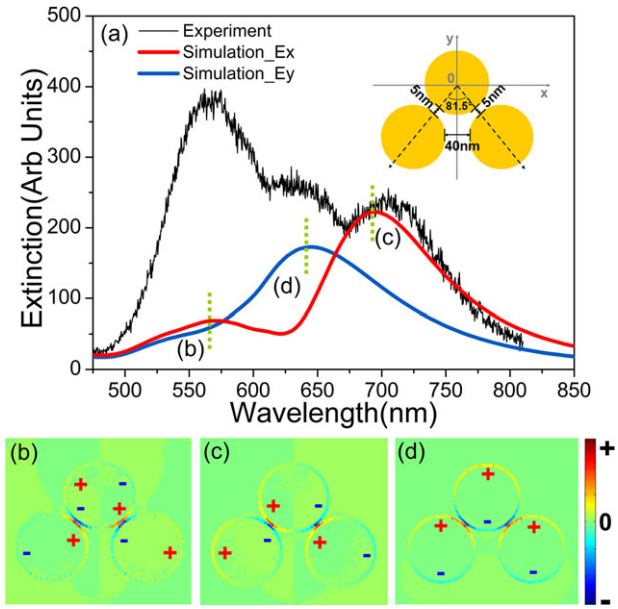

Figure 4 (a) Scattering spectra of the trimer. The experimental result (black) was obtained using unpolarized excitation and the simulated spectra are excited by light linearly polarized along either the *x*-direction (red) or *y*-direction (blue) polarization. The inset illustrates the right-triangle-like trimer consisting of three 110-nm diameter gold nanoparticles. (b)–(d) Calculated surface charge-density distributions for three LSPR modes at the corresponding wavelengths indicated in (a).

Similar results were obtained when the laser at $\lambda = 633$ nm was used to illuminate the trimer, as shown in Fig. 3c. Regarding the spectral dependence of the directivity, this result means that the trimer is able to modify the radiation directivity with a broad spectra bandwidth. After calculation, it is found that the unidirectional scattering exists in the spectral range from $\lambda = 480$ nm to $\lambda = 750$ nm, covering the whole plasmon resonance band of the trimer as indicated in Fig. 4a. In addition to the experiments, the far-field scattering patterns were also calculated by employing the FDTD method and

© 2015 by WILEY-VCH Verlag GmbH & Co. KGaA, Weinheim

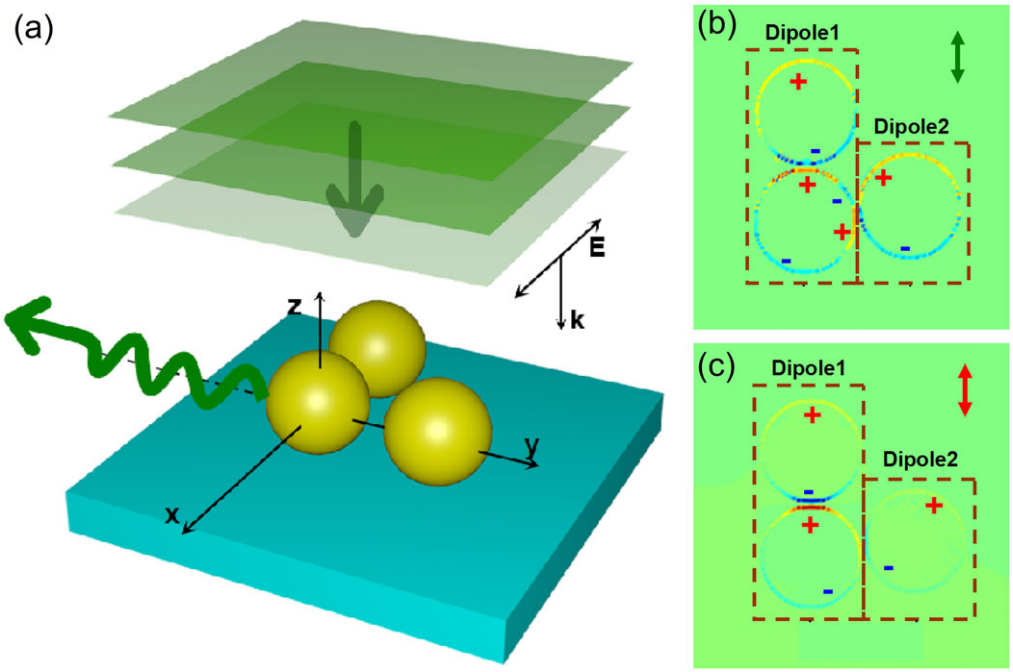

Figure 5 (a) Scheme of calculating the directional scattering by the trimer. (b) and (c) Surface charge-density distributions of the right-triangle-like trimer illuminated at wavelengths of 532 nm and 633 nm, respectively. The two-dipole model was applied based on two areas marked in brown dashed contour.

near-field-to-far-field transformation method. We found that the experimental and simulated results are in agreement with each other qualitatively. It should be noted that there are some deviations between the experimental and simulated results, e.g., the first column of the pattern images in Figs. 3a and b. This could be ascribed to two plausible reasons: the imperfection of the assembled trimer and the error of the optical measurements. The imperfection of the assembled trimer is due to the deviation of the size and shape of the synthesized AuNPs from the ideal sphere shape, and the deviation of the separation and orientation between the coupling AuNPs from the simulation parameters. As for the optical measurements, there could be some experimental errors due to the deviation of the position of the opaque stop in the optical setup and the focus laser spot with respect to the trimer, and the different polarizations of the incident light between the experiment and simulations. All these factors would lead to a deviation between the experimental measurements and the numerical calculations.

To understand the physical origin of directional side scattering by the trimer, the scattering spectrum and the resonant modes were investigated in detail. First, the scattering spectrum of the trimer was measured by a white-light total internal reflection scattering method, as shown in Fig. 4 [50]. The observed scattering spectrum of the trimer, presenting three peaks due to the plasmon coupling, is similar to the previous results [58, 59]. The scattering spectrum of the trimer is calculated by employing the FDTD method. A right-triangle-like configuration with unequal interparticle separations (5 nm, 5 nm, and 40 nm) is modeled, as indicated in the inset of Fig. 4. The simulated spectra are consistent with the experimental observations qualitatively. There is a noticeable deviation between the experimental and simulated spectra at short wavelengths. In addition to the imperfection of the assembled trimer mentioned above, the difference of the excitation light incidence angle could be an important factor, i.e. it is oblique for the experiment but normal for the simulation [47]. To shed light on the resonant modes, the surface charge-density distributions are calculated at different excitation wavelengths, as shown in Figs. 4b–d. As can be seen, for the *x*-direction polarized illumination, the trimer has two hybridized plasmon modes: an inphase electric dipole mode ($\sim$ 696 nm, Fig. 4c) and an antiphase quadrupolar mode ($\sim$ 568 nm, Fig. 4b) due to the strong near-field coupling of the neighboring AuNPs. For the *y*-polarized condition, the trimer exhibits a predominant dipolar resonance peak at $\lambda \sim 643$ nm. The identification of LSPR modes is helpful to understand the plasmonic coupling and provide a phenomenological explanation for the directional scattering.

To further visualize the unidirectional scattering effect, we employed an intuitive phenomenological "two-dipole" model, as discussed previously in the literature [35, 52–54]. Figure 5a shows the model schematically for the directional scattering of the trimer under illumination of a plane wave light. Figures 5b and c show the distributions of surface charge density illuminated with 532-nm and 633-nm light, respectively. In the "two-dipole" model, the right- and left-partial resonators are treated as two coherent electric dipoles oscillating in the *y*-direction as depicted in Figs. 5b and c. The near-field coupling of a quadrupolar mode and two dipolar modes gives rise to the origin of directional

© 2015 by WILEY-VCH Verlag GmbH & Co. KGaA, Weinheim

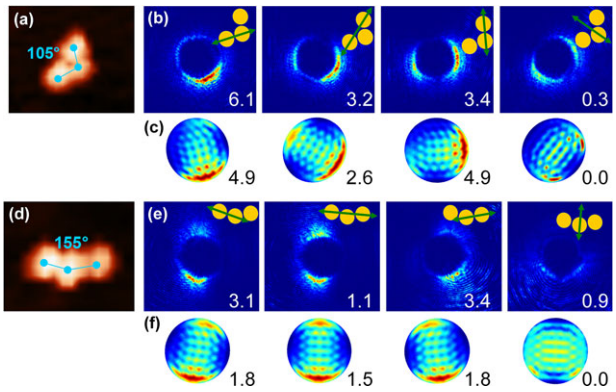

Figure 6 Scattering patterns of plasmonic trimer with different intersection angles: (a)–(c) for $\theta = 105°$ and (d)–(f) for $\theta = 155°$. (a), (d) AFM images of the corresponding trimer configurations. Experimental (b), (e) and simulated (c), (f) pattern images for different incident light polarizations as indicated by the double arrows, respectively. The directivity values are also indicated correspondingly for comparison, and the unit dB is omitted for simplicity.

scattering for the 532-nm light. As for the 633-nm light, the directional scattering is due to the interference of three dipolar modes. For the "two-dipole" model, the interference of two coherent dipoles is determined mainly by two conditions: the total phase difference $\Delta\varphi+kL$ or $\Delta\varphi–kL$, and the amplitudes of dipolar moments. Here, we obtain the relative amplitude and phase difference between the two dipoles according to the surface charge density distribution. Briefly, the total dipole moment $P = pe^{i\varphi}$ is calculated as $P_i(\lambda) = \iint \rho_i(x, y, \lambda) \cdot y dx dy$, where $i = 1, 2$ represents the left or right dipole as shown in Figs. 5b and c, and $\rho_i(x, y, \lambda)$ is the complex charge density. The dipole–dipole separation L is obtained as the weighted average of the x-coordinate value with the weight of $D_i(x) = \int \rho_i(x, y, \lambda) \cdot y dy$. For the 532-nm excitation, the calculation result shows that the dipolar phase difference $\Delta\varphi$ is 1.163π with $kL = 0.157\pi$ ($L = 20.9$ nm) and $p_1/p_2 = 1.26$. So that the total phase difference in the $+x$-direction is $\Delta\varphi - kL = 1.006\pi$, resulting in destructive interference, which almost suppresses the radiation completely in the $+x$-direction. For the 633-nm illumination case, the phase difference becomes to 1.067π, with $kL = 0.077\pi$ (here, $L = 12.2$ nm) and $p_1/p_2 = 1.19$. Hence, the total phase difference in the $+x$-direction becomes 0.99π with a similar dipolar amplitude, leading to unidirectional light scattering as well. This analysis explains intuitively the origin of the directional scattering directivity that is due to the interference between multiple LSPR modes of the asymmetrical oligomer.

Furthermore, as demonstrated theoretically in Fig. 1, the trimers with different configurations would also present unidirectional scattering. Taking the advantages of AFM nanomanipulation, the assembled trimer was adjusted slightly for different configurations, as illustrated in Fig. 1b. As the AFM images in Figs. 6a and d show, we obtain another two representative trimer configurations with the intersection angles $\theta = 105°$ and $\theta = 155°$, respectively. Figures 6b and e present the corresponding experimental radiation patterns excited at a wavelength of 532 nm with different incident-light polarizations. Similar to the above right-triangle-like configuration, an obvious unidirectional side scattering of light occurs when the incident light polarizes along one side of the trimer. Also, the scattering intensity distribution shows two symmetric weaker lobes as the light polarize parallel to the symmetry axis of the

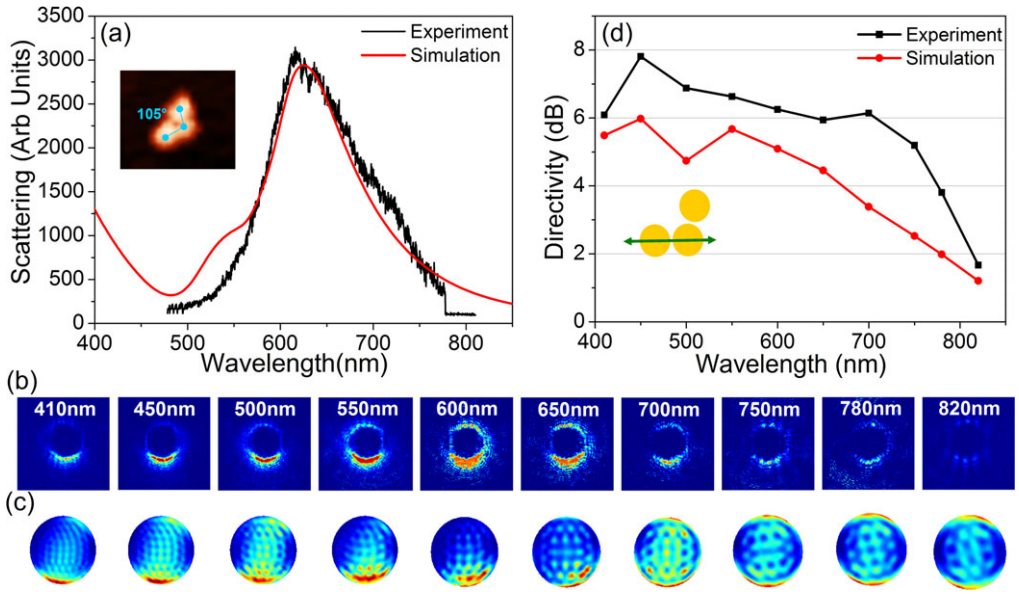

Figure 7 Spectra dependence of directional side scattering by the $\theta = 105°$ trimer. (a) Experimental and simulated scattering spectra of the trimer. Experimental (b) and simulated (c) scattering patterns of the trimer excited at different wavelengths from 410 nm to 820 nm. (d) Calculated and experimental directivity of the trimer at different wavelengths.

© 2015 by WILEY-VCH Verlag GmbH & Co. KGaA, Weinheim

trimer. We also compared the experimental directivity of the two situations and obtained directivity ∼ 6.1 dB for the $\theta = 105°$ trimer, and directivity ∼3.4 dB for the $\theta = 155°$ one. The directivity of the $\theta = 155°$ trimer is relative weak, which is in agreement with the simulated results shown in Fig. 1, and the scattered light intensity decreases clearly due to weak light coupling efficiency when the incident light polarization is parallel to the symmetry axis of the trimer. In short, all experimental and corresponding simulated patterns shown in Figs. 3 and 6 demonstrate that unidirectional light scattering is achievable by different trimers when their configurations are asymmetrical relative to the light polarization.

Moreover, we investigate the spectral dependence of the scattering directivity by using a supercontinuum source (EXB-6, NKT photonics) with a tunable wavelength filter. The incident-light polarization is along one side of the trimer at different wavelengths ranging from 410 nm to 820 nm. The experimental and simulated scattering spectra of the $\theta = 105°$ trimer are shown in Fig. 7a. The experimental far-field scattering patterns are displayed in Fig. 7b and the corresponding simulated scattering patterns are shown in Fig. 7c, presenting a good agreement with each other. Obviously, unidirectional scattering occurs in a broad spectral range. To quantify the directionality of each excitation condition, we summarize the directivities for both the experimental and the simulated patterns in Fig. 7d. The experimental directivity reaches a maximum of ∼7.82 dB when the incident light is at a wavelength of 450 nm, whereas the directivity decreases rapidly if $\lambda > 750$ nm. Directional scattering is achievable ranging from $\lambda \sim 410$ nm to 750 nm with a high directional scattering contrast. Such an ultracompact trimer nanoantenna can modify the emission direction with a broad spectra response effectively.

5. Conclusion and outlook

In summary, we utilized the AFM manipulation method to assemble colloid gold nanoparticles to construct plasmonic oligomers. The directional scattering properties of the plasmonic oligomers were investigated from single nanoparticle monomers, dimers, to trimers. Unidirectional side scattering in the direction perpendicular to the incident light polarization was observed for the trimer with the directivity up to ∼7.8 dB in experiments. The trimers with different intersection angles demonstrate the ability of unidirectional scattering with a broad response bandwidth over 400 nm. The FDTD simulations and a phenomenological "two-dipole" model were employed to understand the scattering patterns. Through plasmon-mode analysis, we ascribe the unidirectional light scattering effect to the interference between the dipolar and quadrupolar LSPR modes due to the AuNPs' near-field coupling. Such a plasmonic directional antenna is a promising platform for ultracompact directional emission manipulation in a photonic circuit. These findings also contribute to optimizing nanoantenna performances for practical applications, e.g. increasing the detection efficiency of surface-enhanced spectroscopy. The conventional "hot spots" within colloids aggregations or rough metal films substrate should not only enhance the signal intensity but also modify the emission direction. The present observations of the trimer are helpful for understanding and manipulating surface-enhanced spectroscopy.

Supporting Information

Additional supporting information may be found in the online version of this article at the publisher's website.

Acknowledgements. This work was supported by the National Key Basic Research Program of China (grant nos.2013CB328703) and the National Natural Science Foundation of China (grant nos. 61422502, 11374026, 91221304, 11121091).

Received: 11 April 2015, **Revised:** 29 June 2015,
Accepted: 15 July 2015

Published online: 21 August 2015

Key words: directional scattering, nanoantenna, nanomanipulation, assembly, atomic force microscope.

References

[1] J. A. Schuller, E. S. Barnard, W. Cai, Y. C. Jun, J. S. White, and M. L. Brongersma, Nature Mater. **9**, 193–204 (2010).
[2] N. Engheta, Science **334**, 317–318 (2011).
[3] L. Novotny and N. Van Hulst, Nature Photon. **5**, 83–90 (2011).
[4] D. K. Gramotnev and S. I. Bozhevolnyi, Nature Photon. **4**, 83–91 (2010).
[5] J. N. Anker, W. P. Hall, O. Lyandres, N. C. Shah, J. Zhao, and R. P. Van Duyne, Nature Mater. **7**, 442–453 (2008).
[6] M. Moskovits, Rev. Mod. Phys. **57**, 783 (1985).
[7] W. L. Barnes, A. Dereux, and T. W. Ebbesen, Nature **424**, 824–830 (2003).
[8] H. X. Xu, J. Aizpurua, M. Käll, and P. Apell, Phys. Rev. E **62**, 4318 (2000).
[9] A. Kinkhabwala, Z. F. Yu, S. H. Fan, Y. Avlasevich, K. Müllen, and W. E. Moerner, Nature Photon. **3**, 654–657 (2009).
[10] G. Lu, L. Hou, T. Zhang, W. Li, J. Liu, P. Perriat, and Q. Gong, J. Phys. Chem. C **115**, 22877–22885 (2011).
[11] O. M. Maragò, P. H. Jones, P. G. Gucciardi, G. Volpe, and A. C. Ferrari, Nature Nanotechnol. **8**, 807 (2013).
[12] L. Tong, V. D. Miljkovic, P. Johansson, and M. Käll, Nano Lett. **11**, 4505–4508 (2011).
[13] A. S. Urban, A. A. Lutich, F. D. Stefani, and J. Feldmann, Nano Lett. **10**, 4794–4798 (2010).
[14] Y. C. Jun, K. C. Y. Huang, and M. L. Brongersma, Nature Commun. **2**, 283 (2011).
[15] H. Shen, G. Lu, T. Zhang, J. Liu, Y. He, Y. Wang, and Q. Gong, J. Opt. Soc. Am. B **30**, 2420 (2013).
[16] H. Aouani, O. Mahboub, N. Bonod, E. Devaux, E. Popov, H. Rigneault, T. W. Ebbesen, and J. Wenger, Nano Lett. **11**, 637–644 (2011).

© 2015 by WILEY-VCH Verlag GmbH & Co. KGaA, Weinheim

[17] A. Ahmed and R. Gordon, Nano Lett. **12**, 2625–2630 (2012).
[18] C. Sonnichsen, B. M. Reinhard, J. Liphardt, and A. P. Alivisatos, Nature Biotechnol. **23**, 741–745 (2005).
[19] P. Nordlander, C. Oubre, E. Prodan, K. Li, and M. I. Stockman, Nano Lett. **4**, 899–903 (2004).
[20] M. Quiten and U. Kreibig, Surf. Sci. **172**, 557–577 (1986).
[21] J. A. Fan, C. H. Wu, K. Bao, J. M. Bao, R. Bardhan, N. J. Halas, V. N. Manoharan, P. Nordlander, G. Shvets, and F. Capasso, Science **328**, 1135–1138 (2010).
[22] A. Artar, A. A. Yanik, and H. Altug, Nano Lett. **11**, 3694–3700 (2011).
[23] B. Ögüt, N. Talebi, R. Vogelgesang, W. Sigle, and P. A. van Aken, Nano Lett. **12**, 5239−5244 (2012).
[24] N. Liu, M. Hentschel, T. Weiss, A. P. Alivisatos, and H. Giessen, Science **332**, 1407 (2011).
[25] D. K. Lim, K. S. Jeon, H. M. Kim, J. M. Nam, and Y. D. Suh, Nature Nanotechnol. **9**, 60 (2010).
[26] M. P. Busson, B. Rolly, B. Stout, N. Bonod, and S. Bidault, Nature Commun. **3**, 962 (2012).
[27] S. J. Barrow, X. Wei, J. S. Baldauf, A. M. Funston, and P. Mulvaney, Nature Commun. **3**, 1275 (2012).
[28] Z. Li, T. Shegai, G. Haran, and H. Xu, ACS Nano **3**, 637–642 (2009).
[29] T. H. Taminiau, F. D. Stefani, F. B. Segerink, and N. F. Van Hulst, Nature Photon. **2**, 234 (2008).
[30] D. Vercruysse, X. Zheng, Y. Sonnefraud, N. Verellen, G. Di Martino, L. Lagae, A. E. Vandenbosch, V. Moshchalkov, S. Maier, and P. Van Dorpe, ACS Nano **8**, 8232–8241 (2014).
[31] I. M. Hancu, A. G. Curto, M. Castro-López, M. Kuttge, and N. F. van Hulst, Nano Lett. **14**, 166–171 (2013).
[32] G. Pellegrini, P. Mazzoldi, and G. Mattei, J. Phys. Chem. C **116**, 21536−21546 (2012).
[33] W. Liu, A. E. Miroshnichenko, D. N. Neshev, and Y. S. Kivshar, ACS Nano **6**, 5489−5497 (2012).
[34] N. S. King, Y. Li, C. Ayala-Orozco, T. Brannan, P. Nordlander, and N. J. Halas, ACS Nano **5**, 7254–7262 (2011).
[35] D. Vercruysse, Y. Sonnefraud, N. Verellen, F. B. Fuchs, G. Di Martino, L. Lagae, V. V. Moshchalkov, S. A. Maier, and P. Van Dorpe, Nano Lett. **13**, 3843–3849 (2013).
[36] Y. H. Fu, A. I. Kuznetsov, A. E. Miroshnichenko, Y. F. Yu, and B. Lukyanchuk, Nature Commun. **4**, 1527 (2013).
[37] T. Coenen, F. B. Arango, A. F. Koenderink, and A. Polman, Nature Commun. **5**, 3250 (2014).
[38] T. Coenen and A. Polman, ACS Nano **8**, 7350–7358 (2014).
[39] E. Le Moal, S. Marguet, B. Rogez, S. Mukherjee, P. Dos Santos, E. Boer-Duchemin, G. Comtet, and G. Dujardin, Nano Lett. **13**, 4198−4205 (2013).
[40] M. V. Rybin, P. V. Kapitanova, D. S. Filonov, A. P. Slobozhanyuk, P. A. Belov, Y. S. Kivshar, and M. F. Limonov, Phys. Rev. B **88**, 205106 (2013).
[41] A. G. Curto, G. Volpe, T. H. Taminiau, M. P. Kreuzer, R. Quidant, and N. F. van Hulst, Science **329**, 930−933 (2010).
[42] T. Kosako, Y. Kadoya, and H. F. Hofmann, Nature Photon. **4**, 312−315 (2010).
[43] D. Dregely, R. Taubert, J. Dorfmüller, R. Vogelgesang, K. Kern, and H. Giessen, Nature Commun. **2**, 267 (2011).
[44] I. S. Maksymov, I. Staude, A. E. Miroshnichenko, and Y. S. Kivshar, Nanophotonics **1**, 65−81 (2012).
[45] M. Barth, S. Schietinger, S. Fischer, J. Becker, N. Nüsse, T. Aichele, B. Löchel, C. Sönnichsen, and O. Benson, Nano Lett. **10**, 891–895 (2010).
[46] R. Resch, A. Bugacov, C. Baur, B. E. Koel, A. Madhukar, A. A. G. Requicha, and P. Will, Appl. Phys. A **67**, 265–271 (1998).
[47] F. Shafiei, F. Monticone, K. Q. Le, X. X. Liu, T. Hartsfield, A. Alù, and X. Li, Nature Nanotechnol. **8**, 95–99 (2013).
[48] S. Kim, F. Shafiei, D. Ratchford, and X. Li, Nanotechology **22**, 115301 (2011).
[49] G. Frens, Nature **241**, 20–22 (1973).
[50] T. Zhang, H. Shen, G. Lu, J. Liu, Y. He, Y. Wang, and Q. Gong, Adv. Opt. Mater. **1**, 335–342 (2013).
[51] C. Huang, A. Bouhelier, G. C. Des Francs, A. Bruyant, A. Guenot, E. Finot, L.-C. Weeber, and A. Dereux, Phys. Rev. B **78**, 155407 (2008).
[52] B. Rolly, B. Stout, S. Bidault, and N. Bonod, Opt. Lett. **36**(17), 3368–3370 (2011).
[53] B. Rolly, B. Stout, and N. Bonod, Phys. Rev. B **84**(12), 125420 (2011).
[54] T. Shegai, S. Chen, V. D. Miljković, G. Zengin, P. Johansson, and M. Käll, Nature Commun. **2**, 481 (2011).
[55] A. Weigel, A. Sebesta, and P. Kukura, ACS Photon. **1**, 848–856 (2014).
[56] B. Sick, B. Hecht, and L. Novotny, Phys. Rev. Lett. **85**, 4482 (2000).
[57] N. Hartmann, G. Piredda, J. Berthelot, G. C. Francs, A. Bouhelier, and A. Hartschuh, Nano Lett. **12**, 177–181 (2011).
[58] S. J. Barrow, A. M. Funston, X. Wei, and P. Mulvaney, Nano Today **8**, 138–167 (2013).
[59] L. Chuntonov and G. Haran, Nano Lett. **11**, 2440–2445 (2011).

© 2015 by WILEY-VCH Verlag GmbH & Co. KGaA, Weinheim